Discover Chemical Engineering

Research

Optimization study on thermal performance of a novel dynamic phase change material wall

Guixiao Zhang[1] · Yuyu Min[1] · Dengyue Chen[2] · Meng Wang[1] · Bing Wang[1]

Received: 18 October 2023 / Accepted: 10 January 2024
Published online: 18 January 2024

Abstract
A new concept of dynamic phase change material (PCM) wall structure in building envelope is proposed to enhance the passive solar energy utilization, in which PCM wall position could be exchanged with insulation layer. The thermal performance of phase change materials in buildings is related to many factors. To ensure that the novel dynamic PCM wall structure could reach its full potential, the thermal performance of the structure was numerically simulated and optimized based on different climatic conditions, room sizes and the position of PCM layer in the wall. The results indicated that the suitable PCM was different when using the novel dynamic PCM wall in different climates. Among the four cities of Harbin, Tianjin, Jinan and Guangzhou, northern cities, like Tianjin, were more suitable for using PCM A16 than southern cities. In terms of room size design, when the volume of the room remained identical, the room size design formed a certain correlation with the indoor temperature. In addition, results showed that the location of the novel PCM wall system in the wall would cause a great difference in indoor temperature, which was related to heat dissipation at different locations.

Keywords Optimization · PCM · CFD · Dynamic PCM wall · Thermal performance

List of symbols

v	Fluid velocity (m/s)
h	Sensible enthalpy (J/kg)
c_p	Specific heat capacity [J/ (kg K)]
k	Turbulence kinetic energy
g	Gravitational acceleration (m/s^2)
H	Enthalpy (J/kg)
K	Thermal conductivity [W/ (m·K)]
S	Source term
L	Latent heat (J/kg)
T	Temperature (K)
S_h	Volumetric heat source term
P	Pressure (Pa)
F	External force (N)
C_μ	Coefficient, a function of the mean strain, rotation and turbulence fields

Guixiao Zhang and Yuyu Min contributed equally to this work.

✉ Bing Wang, bwang@nankai.edu.cn | [1]College of Environmental Science and Engineering/Sino-Canada Joint R&D Centre for Water and Environmental Safety, Nankai University, Tianjin 300071, People's Republic of China. [2]School of Pharmaceutical Sciences, Xiamen University, Xiamen 361005, Fujian, China.

G_k Turbulence kinetic energy due to the mean velocity gradients
G_b Turbulence kinetic energy due to buoyancy
J_j Diffusion flux

Greek symbols
ρ Density (kg/m^3)
β Liquid fraction
ε Dissipation rate

Subscripts
ref Reference
m Melting point
eff Effective
t Turbulence

1 Introduction

As International Energy Agency [1] reports, building and the construction sector takes up nearly 40% of greenhouse gas emission. The appropriate designs of building envelop needs to be exploit for their energy saving potential [1]. Phase Change Material (PCM) is comprising material, which could be placed in walls to capture and store passive solar energy instead of conventional energy to heat buildings [2–6].

Early studies from 1990s by Athienitis et al. which reduced room peak temperature by 4 ℃ [7], indicated its attractiveness of reducing temperature fluctuation inside buildings. In order to further improve energy efficiency of PCMs, much research has focused on its structure and thermal performance for application [8–10]. Izquierdo-Barrientos et al. [11] and Lagou et al. [12] installed PCM board on internal side, external side and other positions of building envelope to obtain approximate phase transition temperature range for each configuration and different European locations. Jin et al. [13] determined the optimal location of PCM by 1/5 distance from the bounding wallboard of buildings, to obtain the least PCM temperature fluctuation. Yu et al. [14] placed the PCMs on outer wall surface to facilitate the release of PCM solidification heat during summer nights.

Furthermore, Gracia proposed a dynamic system in which the position of PCM relative to the insulation can be changed [15], which can ensure that peak cooling load can be discharged to outdoors without obstruction of insulation layer. The PCM was 7 mm thickness, due to its specific rotating structure, PCM wall can't be too thick due to position exchange. So it was probably proposed to use in Spain climate of summer [15]. While the dynamic PCM system in current work was for cold winter. Moreover, different structure was designed and much thicker PCM wall was adopted for winter application. And the thermal performance for heat transferred into interior room was analyzed and economic potential was also evaluated.

In general, the thermal performance of entire building caused by PCM heat exchange is complex, which involved coupled heat and air flow. The possibility to obtain temperature contour distribution in entire space by experiments is highly limited, hence numerical simulation method is a very useful tool to explore the complicate thermal behavior of PCM system in buildings [16–18]. Jin and Zhang [19] built a numerical model of double layer PCM floor, which showed about 40% energy release shift from peak period and mitigated temperature fluctuation. Markarian et al. [20] adopted a multi-objective algorithmic programs to simulate and evaluate the economic benefits and carbon emissions brought by different PCM types and locations in five cities in Iran. Moreover, Computational Fluid Dynamics (CFD) is a powerful tool for understanding the heat transfer regime and air flow by characterizing PCM phase change through solving mathematical equations [21]. Mahdaoui et al. [22] used Ansys Fluent software to assess the thermal performance and turned out that the addition of PCM into hollow brick played a vital role in reducing indoor temperature swing.

Hence, the position of PCM and insulation layer are significant for thermal performance and energy saving, which needs further optimization. To counter those drawbacks, an innovative design of dynamic PCM system was proposed in current work, and CFD simulation was used to evaluate its application potential. Unfortunately, limited research concerning some of the problems faced in application of this new PCM system has taken place. Questions remaining include: (i) According to different place and weather, the heat effect from the system is unknown; (ii) For different room size, the heat effect need to be optimized; (iii) the heat effect from different position of PCM should be considered.

In this work, a dynamic PCM wall system was optimized, in which the position of PCM can be exchanged with insulation during day and night. CFD simulation was conducted by applying the novel PCM wall to a building under realistic ambient temperature and solar radiation. The thermal performance of dynamic PCM wall adopted in building in cold season was evaluated. Based on the novel dynamic PCM wall, the numerical simulation was carried out in four cities of Harbin, Tianjin, Jinan and Guangzhou in China. In order to maximize energy saving, the climate condition, room size and the position of the novel dynamic PCM wall system in the south wall were optimized.

2 Description of the model

2.1 Proposed wall system

As shown in Fig. 1a, the conceptual architecture of target room which was southernly exposure in a building in Northern hemisphere. As shown in Fig. 2(a), the size of the room is $5.2 \times 3.75 \times 2.6$ m, while the PCM is placed in the part of the wall below the window opening with surface area of 1.0×0.8 m^2. In multi-story buildings, it can be placed inside the spandrel walls. In order to conveniently exchange the position of PCM and insulation layers, and without break the wall structure of the whole building envelope, the PCM layer and insulation was made in a column of 37.5 mm radius and 800 mm height. According to the room and PCM amount, these columns could be arranged horizontally, as shown in Fig. 1b. In this way, the columns could be rotated to realize the position exchange of PCM and insulation layers, without breaking the building structure.

Referring to Fig. 1b, in the daytime, the PCM layer could be located outside the insulation, to absorb solar radiation more directly and faster, the energy could be stored through PCM melting process. While during the night, it could be rotated to the inside of insulation, the PCM released the discharging heat to the room, which could be dissipated to the external less since the insulation was outside. The melting and solidification process could be influenced by PCM location, thus the energy transferred into the room could be different, which could result in indoor temperature changes. It is important to mention that this study is focused on proof and validation of concept of dynamic PCM wall rather than the mechanics of the PCM rotation the focus of this work was to proof and validate the concept of dynamic PCM wall, rather than the mechanics of rotation. However, by making the PCM-insulation units suitably dimensioned, each unit can be rotated sequentially and automatically by the spindle.

Different layers of building envelop in this study was shown in Fig. 2b. The 4 layers consist of plaster with insulation, backing, PCM and brick with thickness of 20, 50, 25 and 100 mm respectively. The outside brick veneer faces the south as indicated in the figure. The weather used in this work was from the city of Tianjin and Harbin, China, which locations were latitude 39.13 and latitude 45.75 and have cold climate in winter.

2.2 Mathematical model and governing equations

To evaluate the heat transfer between the inside of the room and outside air through the wall, CFD was used and a model of the room (3D) was constructed in the ANSYS FLUENT 14.5 platform. To model the PCM phase change, the enthalpy-porosity concept in FLUENT was applied, which involves a quantity called the liquid fraction, i.e. the fraction of the liquid versus the solid in each cell of the CFD model. The liquid fraction is computed at each iteration, according to the enthalpy balance. The region where the liquid fraction is between 0 and 1 is called the mushy zone. The mushy zone is modeled as a "pseudo" porous medium in which the porosity decreases from 1 to 0 as the material solidifies. When the material has fully solidified in a cell, the cell porosity becomes zero and mass transport through it ceases.

The governing 3D equations of heat and mass transfer and how they are applied in the present model are presented below.

(i) The energy balance equations for solidification/melting:

$$\frac{\partial}{\partial t}(\rho H) + \nabla \bullet \left(\rho \vec{v} H\right) = \nabla \bullet (K \nabla T) + S \tag{1}$$

where ρ is the density, v is the fluid velocity, K is the thermal conductivity, S is the source term and H is the enthalpy, which is defined as the sum of the sensible enthalpy (h) and the latent heat (ΔH) as

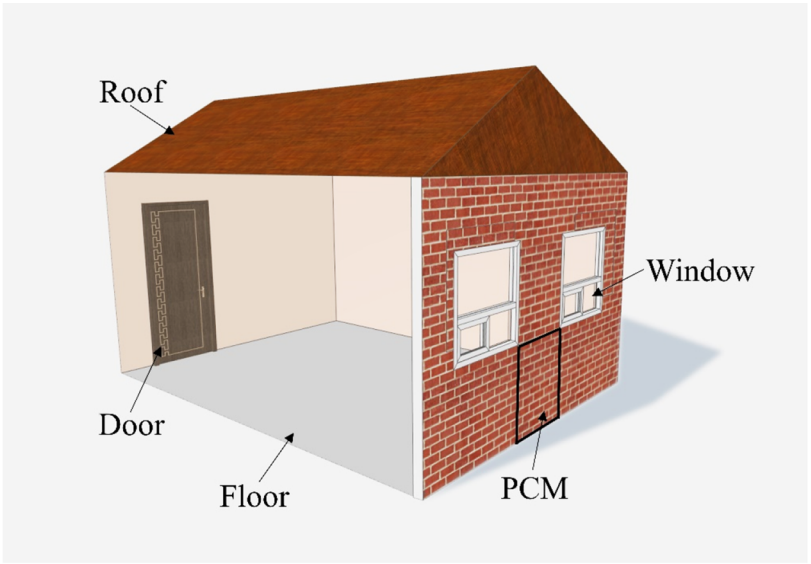

Fig. 1 **a** Room with dynamic PCM wall system; **b** PCM orientations, with Position 1 during daytime, and Position 3 during nighttime

$$H = h + \Delta H \tag{2}$$

where the sensible enthalpy is defined as

$$h = h_{ref} + \int_{T_{ref}}^{T} c_p dT \tag{3}$$

where h_{ref} is the reference enthalpy, T_{ref} is the reference temperature, c_p is the specific heat at constant pressure. The latent heat content ΔH is expressed as

$$\Delta H = \beta L \tag{4}$$

where L is the latent heat of the PCM, and β is its liquid fraction, which can be defined as

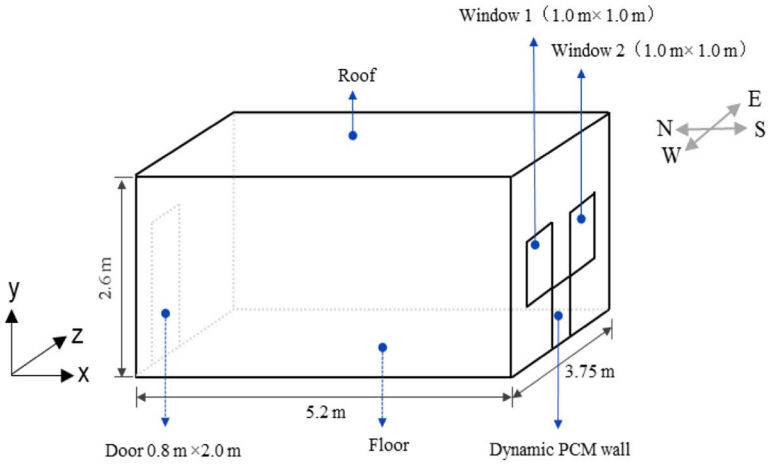

(a)

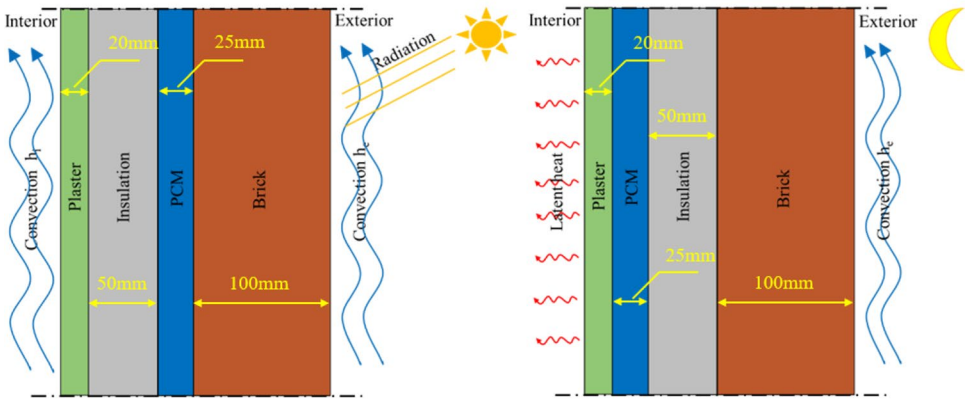

(b)

$$\beta = 0 \quad \text{if} T < T_{liquidus} \tag{5a}$$

$$\beta = 1 \quad \text{if} T < T_{liquidus} \tag{5b}$$

$$\beta = \frac{T - T_{solidus}}{T_{liquidus} - T_{solidus}} \quad \text{if} T_{solidus} < T < T_{liquidus} \tag{5c}$$

To determine the liquid fraction in a mushy zone, in the current analysis a rather small temperature interval ΔT near the PCM melting point (T_m) was selected and it was assumed that melting occurred within a narrow temperature range (T_m-ΔT and $T_m + \Delta T$). Using Eq. (5), and substituting T_m-ΔT and $T_m + \Delta T$ for $T_{solidus}$ and $T_{liquidus}$, respectively, the liquid fraction was calculated [23].

(ii) Heat transfer equation in the solid wall region:

$$\frac{\partial}{\partial t}(\rho h) + \nabla\left(\vec{v}\rho h\right) = \nabla(K\nabla T) + S_h \tag{6}$$

where S_h is the volumetric heat source term. The second term on the left-hand side of Eq. (6) represents convective heat transfer due to rotational or translational motion of the solids. The velocity field is computed from the motion specified for the solid zone as explained in [24]. The terms on the right-hand side of Eq. (6) are the heat flux due to conduction and volumetric heat sources within the solid, respectively.

(iii) The mass and momentum conservation equations for the air flow inside the room:

$$\frac{\partial \rho}{\partial t} + \nabla\left(\rho \vec{u}\right) = 0 \tag{7}$$

$$\frac{\partial}{\partial t}\left(\rho \vec{u}\right) + \nabla\left(\rho \vec{u}\vec{u}\right) = -\nabla P + \rho \vec{g} + \rho \vec{F} + \nabla \vec{\tau} \tag{8}$$

where P, $\vec{g}$ and $\vec{F}$ are the pressure, gravitational acceleration, and external force, respectively.

In FLUENT several turbulence models are available for air flow. The realizable k–ε model was model chosen here for capturing the turbulence of the air movement in the room produced by convective heat transfer. The turbulent viscosity was computed as function of k (turbulence kinetic energy) and ε (energy dissipation rate). Therefore, two additional transport equations for k and ε need be solved, i.e. Equations (9) and (10) as follows

$$\frac{\partial}{\partial t}(\rho k) + \frac{\partial}{\partial x_j}\left(\rho k u_j\right) = \frac{\partial}{\partial x_j}\left[\left(\mu + \frac{\mu_t}{\sigma_k}\right)\frac{\partial k}{\partial x_j}\right] + G_k + G_b - \rho\varepsilon - Y_M \tag{9}$$

$$\frac{\partial}{\partial t}(\rho \varepsilon) + \frac{\partial}{\partial x_j}\left(\rho \varepsilon u_j\right) = \frac{\partial}{\partial x_j}\left[\left(\mu + \frac{\mu_t}{\sigma_\varepsilon}\right)\frac{\partial \varepsilon}{\partial x_j}\right] + \rho C_1 S\varepsilon - \rho C_2 \frac{\varepsilon^2}{k + \sqrt{\upsilon\varepsilon}} + C_{1\varepsilon}\frac{\varepsilon}{k}C_{3\varepsilon}G_b + S_\varepsilon \tag{10}$$

where

$$\mu_t = \rho C_\mu \frac{k^2}{\varepsilon} \tag{11}$$

$$C_1 = \max[0.43, \frac{\eta}{\eta + 5}] \tag{12}$$

$$\eta = S\frac{k}{\varepsilon} \tag{13}$$

$$S = \sqrt{2S_{ij}S_{ij}} \tag{14}$$

In these equations, C_μ is not constant, but is a function of the mean strain, rotation and turbulence fields; G_k represents the generation of turbulence kinetic energy due to the mean velocity gradients; G_b is the generation of turbulence kinetic energy due to buoyancy; Y_M represents the contribution of the fluctuating dilatation in compressible turbulence to the overall dissipation rate; C_2, $C_{1\varepsilon}$ and $C_{3\varepsilon}$ are constants; σ_k and σ_ε are the turbulent Prandtl numbers for k and ε, respectively;S_k and S_ε are user-defined source terms.

The energy balance equation for air flow is

$$\frac{\partial}{\partial t}(\rho E) + \nabla \bullet \left(\vec{v}(\rho E + p)\right) = \nabla \bullet \left(D_{eff}\nabla T - \sum_j h_j \vec{J}_j + \left(\bar{\bar{\tau}}_{eff} \bullet \vec{v}\right)\right) + S_h \tag{15}$$

where $D_{eff} = D + D_t$ is the effective conductivity, D_t is the turbulent thermal conductivity, defined according to the selected turbulence model, and $\vec{J}_j$ is the diffusion flux of species j. The first three terms on the right-hand side of Eq. (15) represent energy due to conduction, species diffusion, and viscous dissipation, respectively while S_h represents the volumetric heat sources. The quantity E is given by

$$E = h - \frac{p}{\rho} + \frac{v^2}{2} \tag{16}$$

The sensible enthalpy h is defined for ideal gases as

$$h = \sum_j Y_j h_j + \frac{p}{\rho} \tag{17}$$

2.3 Material properties

Many studies [25, 26] revealed the benefits of organic PCMs, like paraffin, in building energy saving owing to their superiority of stability and low corrosion [27]. Besides, they are not as prone to supercooling and phase separation as many inorganic PCMs. In present simulation, an organic compound PCM, named A16, was applied to improve building energy efficiency. The relevant properties of PCM A16 and other wall layers composition in the present analyses are summarized in Table 1. It must be noted that the merits and demerits of various PCMs are beyond the scope of the present study, but other references can be made to the literature, e.g. [25], for the choice of the appropriate PCM for a particular application.

2.4 Numerical discretization and analysis

Using a pressure-based solver to carried out the simulations in FLUENT. Pressure implicit splitting of operators (PISO) was used for pressure–velocity coupling. A 2nd order upwind scheme was chosen for the discretization of momentum, k and ε equations. A southern exposure of the PCM wall was assumed. Ambient temperature record was downloaded from China's National Meteorological Science Data Center covering the cities of Harbin and Tianjin. The solar radiation was obtained from ASHRAE [29] database, including diffuse solar irradiation, the direct normal solar irradiation, and the ground reflection. The PCM, layers of plaster, insulation and brick were assumed to be well-distributed throughout the wall while the volumetric expansion of the PCM was ignored. The thermal boundary condition for the other walls of the room, such as ceiling and floor, were assumed to be adiabatic.

2.5 Mesh and grid independency

The 3D geometry of the room was constructed with GAMBIT 2.4.6. The Structured Cooper-type hex mesh was created, consisting of 428,505 nodes 1,250,288 faces and 411,008 cells. The average EquiSize Skew parameter, a key parameter for assessing the mesh quality, ranged from 0 to 1 (0-best; 1-worst).

To ensure that the solution was independent of the adopted grid, grid independence testing was conducted. Three grid sizes were considered: 51,376 (fine), 411,008 (extra fine) and 1,881,375 (extremely fine). Simulations were performed for each grid size and it was discovered that the extra fine and the extremely fine meshes gave practically the same results, therefore, the extra fine mesh was selected for further analysis.

3 Model validation

In order to validate the PCM phase change and heat transfer model used in this work, same method was established and compared by the experimental results from Pasupathy et al. [30]. The outside temperature was shown in Fig. 3a and the indoor temperature is 27 ℃. Additionally, the results from our simulation method were also compared to Pasupathy et al. [30] and Li et al. [28]. Pasupathy et al. [30] work details could be found elsewhere.

To simulate the heat transfer process of Pasupathy et al. [30] work, a room model with a size of 1.22 m × 1.22 m × 2.44 m was established through the Fluent software. According to the experimental settings of Pasupathy et al. [30], the same

Table 1 Properties of PCM and other materials used in the present analyses [28]

Material	Density kg/m^3	Specific Heat J/(kg·K)	Thermal Conductivity W/(m·K)	Latent Heat J/kg	Phase Change Temperature K
Brick	1460	880	1.30	—	—
Plaster	900	1000	0.25	—	—
Insulation (EPS)	30	1380	0.042	—	—
PCM (A16)	800	2300	0.18	213,000	288.15

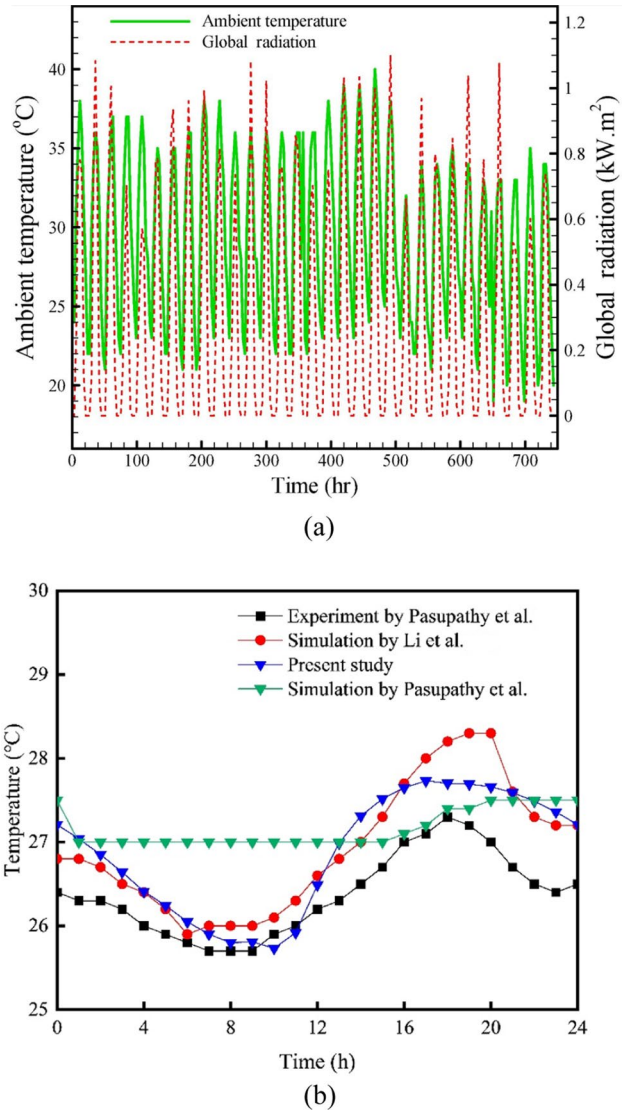

Fig. 3 **a** Temperature distribution and global radiation with respect with respect to time in the summer for the city of Isfahan, Iran [28]; **b** Comparison and validation for the present thermal model with those of Pasupathy et al. [30] and Li et al. [28]

parameters were used in our model method. In compliance with Pasupathy and Li et al. [28, 30] simulations, the convective heat transfer coefficient at the inside and outside surfaces of the roof were 1.0 W/(m^2 K) and 5.0 W/(m^2 K), respectively.

The diurnal temperature variation of the concrete slab soffit obtained by the current simulation are compared with the corresponding experiment values in Fig. 3b. It showed that the simulation results from our thermal model used in this study was agreed with the experimental measurements of Pasupathy et al. [30]. Moreover, it presented closer to the experimental data compared to other simulation results, which indicated the thermal model was robust for the simulation of PCM phase change and its heat transfer process.

4 Results and discussion

4.1 Different climates

According to the different climate characteristics of China, four cities, namely, Harbin, Tianjin, Jinan and Guangzhou, were selected for the simulation analysis. Harbin and Tianjin have a temperate monsoon climate, with cold and dry winters. The difference is that Harbin has higher latitudes and colder winters than Tianjin. Jinan belongs to the warm temperate continental monsoon climate zone, with distinct four seasons and sufficient sunshine, which has the coldest planting season in January throughout the year, with an average temperature of – 0.4 ℃. Guangzhou belongs to the South Asian

tropical monsoon climate zone, with a mild climate and significant maritime climate characteristics. The temperature and solar radiation variation in representative day of each city in February are plotted in Fig. 4a and b, respectively. The outdoor temperature fluctuates from 259 to 272 K, 275 K to 281 K, 276 K to 286 K and 285 K to 298 K in Harbin, Tianjin, Jinan and Guangzhou, separately.

Figure 5 shows the temperature profile and phase change profile of the novel PCM wall system under different climatic conditions. In the simulation of four cities of Harbin, Tianjin, Jinan and Guangzhou, the same PCM A16 was used, and the phase change temperature was fixed at 288.15 K. The dynamic PCM wall system is located on the south facing wall of the room, below the middle of the two windows, as shown in Fig. 1a. In this study, based on the 24-h system, a day is divided into melting (charging) stage and solidification (discharging) stage, which are 08:00–17:00 and 17:00–08:00, respectively. In the melting stage, the hourly temperature distribution of PCM in four cities are shown in Fig. 5a. Accordingly, the phase change process of PCM is shown in Fig. 5b.

As can be seen from Fig. 5a, the temperature of PCM layer at 09:00 in four cities is close to their outdoor temperature. Since their temperature was lower than the phase transition temperature of 288.15 K, they were all in a solidified state. With the increase of ambient temperature and strengthening of solar radiation, the energy obtained by PCM layer also increased, and the temperature rose accordingly. Among the four cities, the temperature of the whole PCM layer in Harbin rose fastest, rising to about 286 K by 12:00, an increase of about 13 K. At about 13:00, the temperature reached the phase change temperature, and the PCM layer began to melt. In the other three cities, the temperature of PCM layer was rising and reaching 288.15 K before 12:00. At 17:00, the temperature of PCM layer in Harbin was still close to the phase change temperature, indicating that it was in the melting state. In the other three cities, the overall temperature of PCM layer at 17:00 was equal to or higher than the phase change temperature, and PCM layer can basically melt completely.

PCM phase transition process during the charging period can also refer to the profile of liquid fraction in Fig. 5b. When the liquid fraction is 0, the picture is blue and PCM is solid phase. On the contrary, when the liquid fraction is 1, the picture is red and PCM is liquid phase. When the liquid fraction is between 0 and 1, the color in the middle of the two indicates that PCM is in paste. It can be seen from Fig. 5b that in Harbin, the PCM begins to melt after 12:00, and about 70% of them melt at 17:00. In the other cities, the PCM layer can almost melt completely before 17:00. In general, PCM in Harbin can not completely melt, which is not conducive to subsequent solidification and heat release, while PCM in Tianjin, Jinan and Guangzhou can almost melt all, which is conducive to solidification and heat release at night.

According to the concept of dynamic PCM wall, after the charging period, the PCM layer will rotate, the insulation layer will face the brick layer, and the PCM will face the room. In the solidification stage, the hourly temperature and liquid phase ratio of PCM in four cities are shown in Fig. 5c and d. At the beginning, the temperature of PCM layer in Harbin did not decrease with the sun setting and the decrease of external temperature. In fact, when PCM layer turned over to the inner side of the wall, the temperature of the solid part facing the insulation and brick layer is low, it can absorb the heat of the brick, so that it continued to melt. At 19:00, the whole PCM layer completely melted. Then, affected by the decrease of external temperature, the temperature of the south side of PCM decreased, so it began to solidify from the

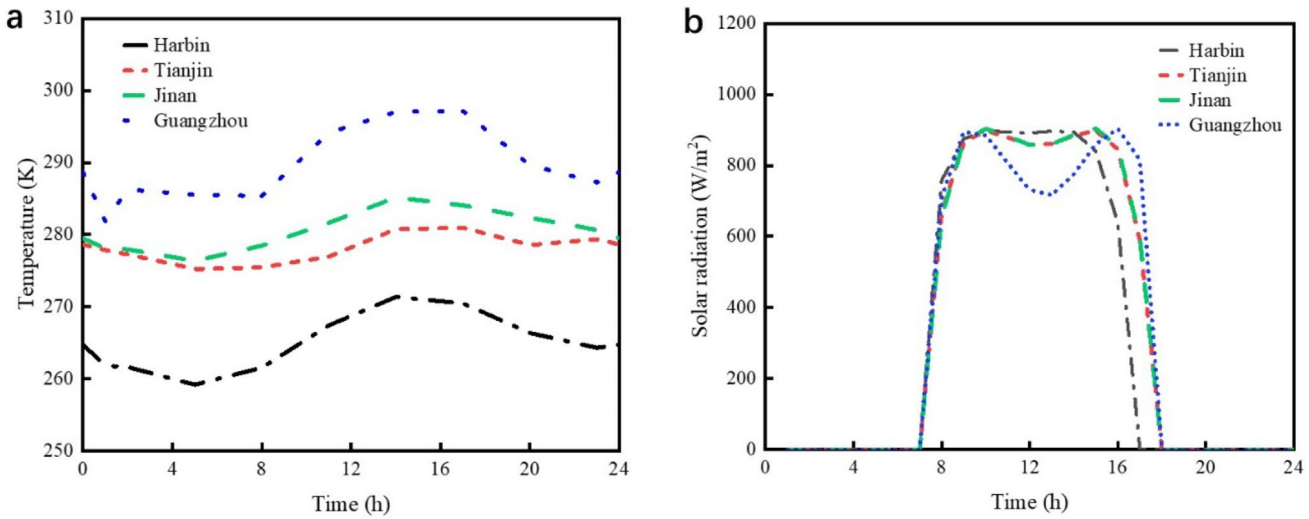

Fig. 4 Meteorological data for (**a**) exterior ambient temperature and (**b**) solar radiation in four cities in China

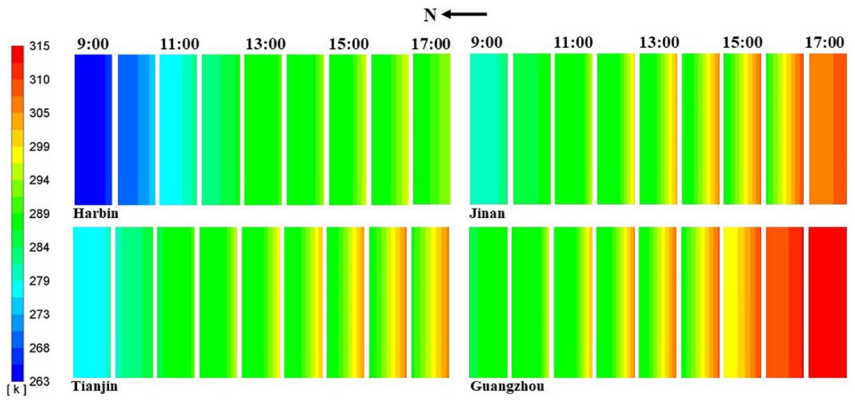

(a) PCM temperature distribution during the thermal charging period.

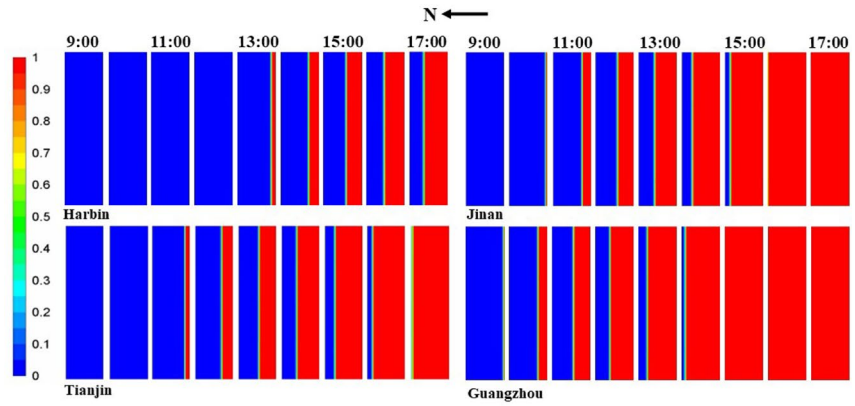

(b) PCM liquid fraction during the thermal charging period.

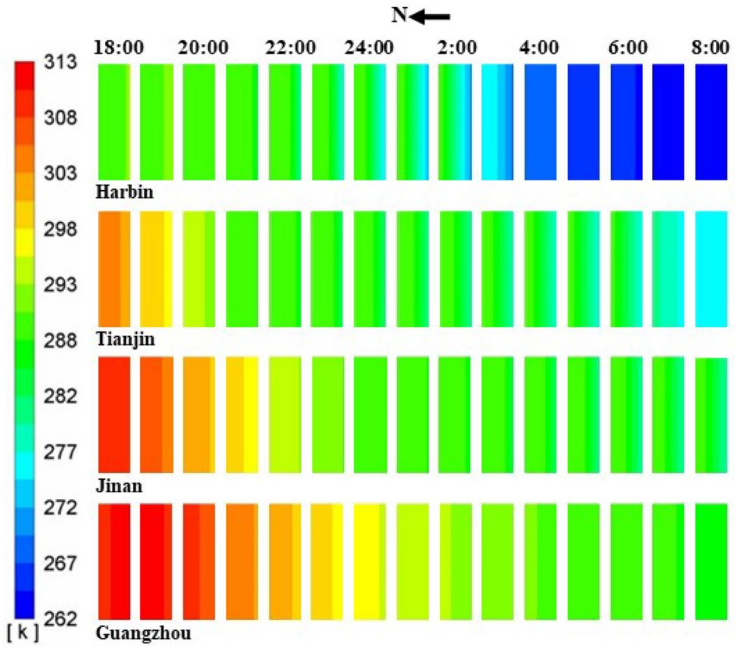

(c) PCM temperature distribution during the discharge period.

Fig. 5 PCM temperature distribution and liquid fraction in the dynamic PCM walls under different climates

Fig. 5 (continued)

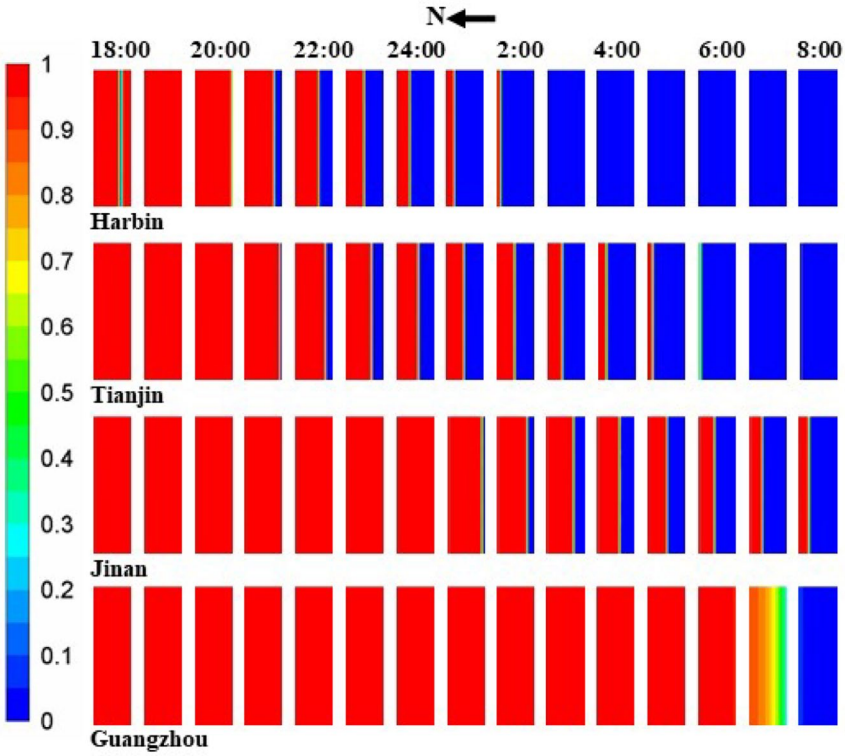

(d) PCM liquid fraction during the discharge period.

south side. Until 03:00, PCM layer completely solidified. In other cities, the temperature of PCM layer decreased at the beginning of solidification stage. Under the influence of the external temperature, the temperature of the south side of the PCM layer decreased faster than that of the north side, so it began to solidify from the south side. In Tianjin, the PCM layer solidified completely at 05:00. In Jinan, the PCM layer solidified about 80% at 08:00. In Guangzhou, there is no solidification of PCM and no energy release during most of the night. Therefore, comparing the solidification heat release in four cities, it was found that when A16 was applied in northern cities, especially in Tianjin, the solidification process had longer heat release time. Further research is needed in Harbin or Jinan by adjusting the thickness and position of A16 or other factors, to improve the thermal performance.

Figure 6 shows the indoor temperature under different climatic conditions during charge and discharge period. During the heat storage stage, the initial indoor temperature is maintained at 298.15 K under the regulation of the HVAC system. It did not rise significantly in the next two hours. At 11:00, with the increase of solar radiation intensity, the indoor temperature in Harbin, Tianjin and Jinan began to increase significantly, and the temperature in Tianjin increased faster than that in Jinan and Harbin, which is influenced by the combined action of solar radiation and external temperature. After 11:00, the room temperature basically maintained the same rising speed. The indoor temperature in Guangzhou has been rising slowly. After 15:00, the rising speed became faster and the temperature finally reached about 301 K. This is mainly due to the rapid enhancement of solar radiation at this time.

During the heat release period, the indoor temperature in Harbin, Tianjin and Jinan was relatively stable in the first six hours, while that in Guangzhou decreased rapidly. In Harbin, after 23:00, the PCM was still solidifying, so it continued to release heat to maintain the indoor temperature unchanged. After two hours, the PCM is basically completely solidified and no longer gives off heat, the indoor temperature drops rapidly. In Tianjin, the solidification of PCM continued until 6 a.m., so it has been supplying heat to the room, and the room temperature can be maintained at about 300 K. After 6:00, PCM was completely solidified and the room temperature decreased briefly. In Jinan, since the PCM is mainly solidified after 1:00, it can also maintain a high temperature. In Guangzhou, PCM basically did not solidify due to the high external temperature. The room temperature basically changed with the ambient temperature and remained at about 290 K.

Comparing the room temperature changes of the four cities, it is found that the temperature in Tianjin can fluctuate around 300 K, which is close to the thermal comfort temperature. For the last three cities, the conditions need to be optimized to improve indoor comfort, such as changing the type of PCM.

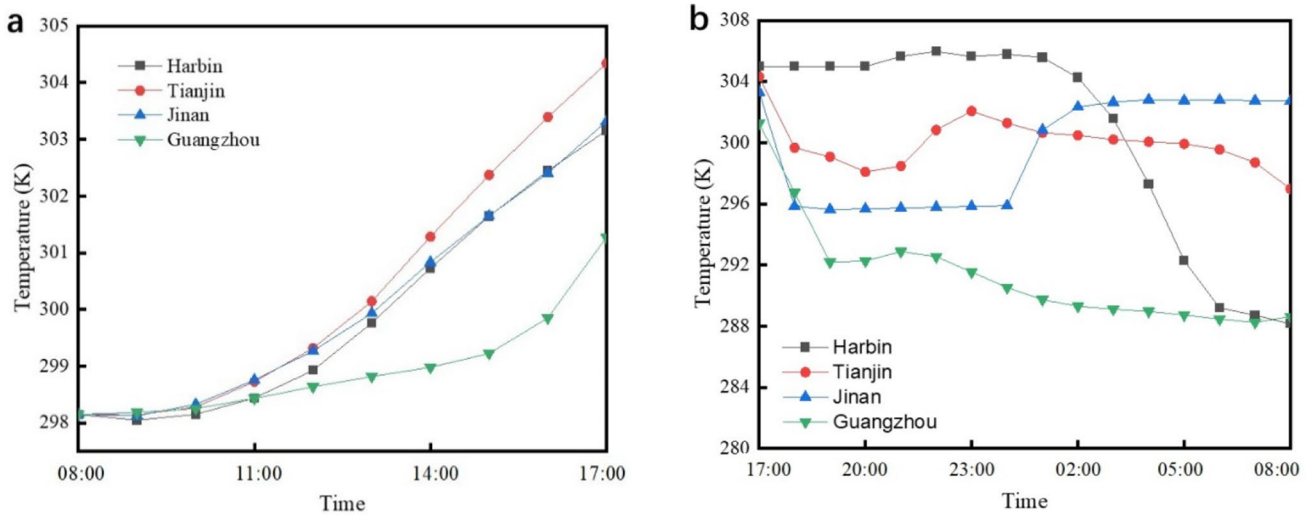

Fig. 6 Room temperature in the dynamic PCM walls under different climates

4.2 Size of room

The numerical simulations were performed for rooms of four sizes (same volume) to study the effect of size on the thermal performance of dynamic PCM wall. The four sizes are 6 m × 3.25 m × 2.6 m (R1), 5 m × 3.9 m × 2.6 m (R2), 4 m × 4.875 m × 2.6 m (R3), 3 m × 6.5 m × 2.6 m (R4), respectively. Based on the research on thermal properties of PCM A16 in different climates in 4.1, Tianjin was selected as the research site. On account of climate conditions of Tianjin in February, PCM solidification process at night and the thermal insulation effect of the room were studied. In order to clearly show the change trend of room temperature, temperature of the center point of room was plotted in Fig. 7. As shown in Fig. 7, the temperature trends of the four cases were consistent. After 20:00, the indoor temperature dropped suddenly, because the latent heat released by PCM was very few, and there was energy loss in the process of diffusion. Then, as the latent heat released increased and the heat diffused, the room temperature began to rise. At 23:00, it reached the highest value, and then began to decline. At 06:00 in the morning, the solidification was over, the heat release was completed, and the temperature dropped faster.

Figure 8 shows 2D profile of temperature in four different sizes of rooms in Tianjin, and the position of the plane in 3D room is shown in Fig. 9. According to Fig. 5b, under the Tianjin climate, there was no heat release from 17:00 to 20:00, so HVAC system was turned on for heating during this period, and the temperature maintained at 303 K. In the next four

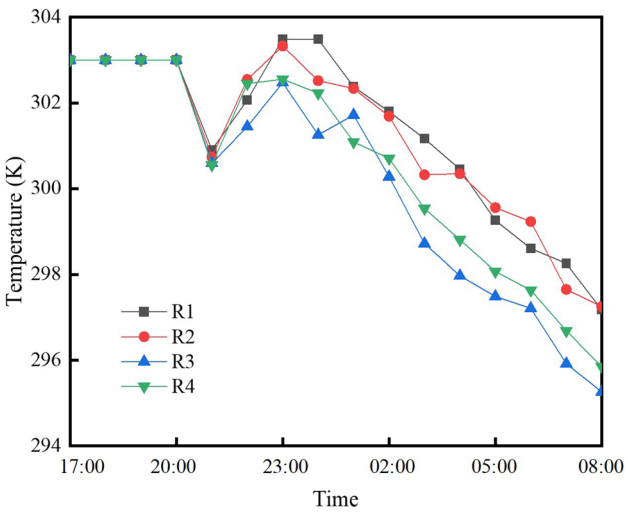

Fig.7 Central point temperature of rooms of different sizes in Tianjin

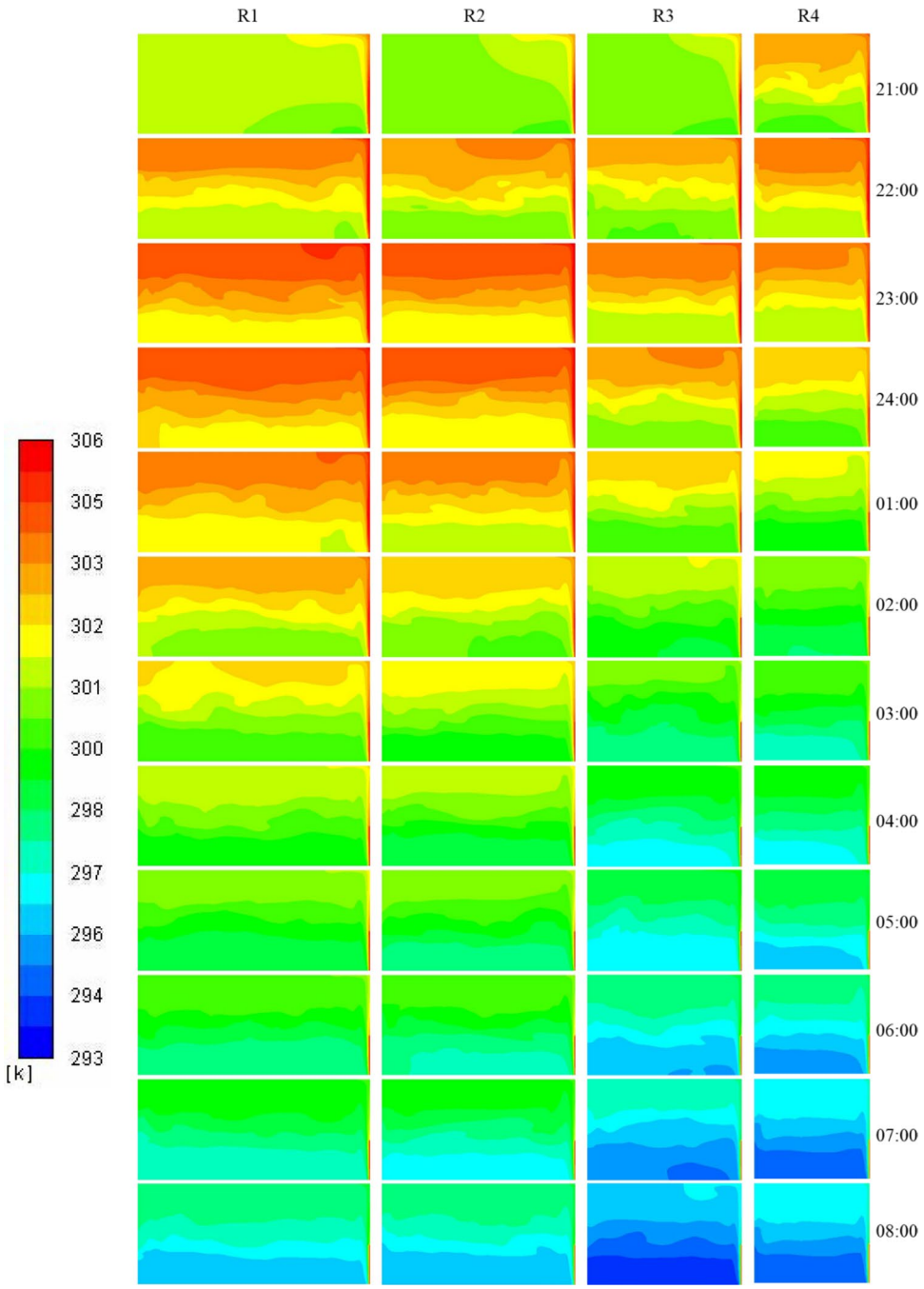

Fig.8 2D profile of temperature in four different sizes of rooms in Tianjin

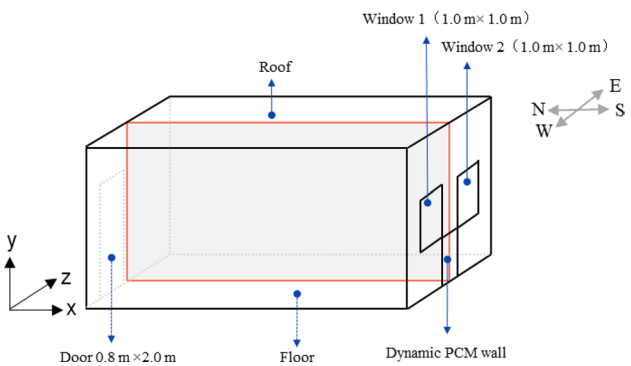

Fig. 9 The position of 2D plane in the room

hours, the heat released by PCM gradually spread, and the room temperature began to rise. The temperature of R1 and R2 locally reaches 305–306 K at 23:00. By 06:00 in the morning, PCM was solidifying, but the heat released was reduced, and the room temperature was decreased. From 06:00 to 08:00, PCM solidified completely, and no longer released heat, so that the room temperature naturally decreased. In the above four cases, the initial temperature of R4 was obviously higher than that of R1, R2 and R3 because of the smallest length of R4 in the cross section shown. In the four cases, the overall temperature from large to small is R1, R2, R3 and R4. That is, the temperature distribution in the room is related to the shape of the room when the volume of the room is the same and other conditions are fixed.

4.3 Position of the PCM layer

The location of the novel dynamic PCM wall system in the south wall of the room was considered to optimize. Figure 10a–e respectively shows five different positions of the novel PCM wall on the south wall of the room. In this study, the novel dynamic PCM wall is 0.8 m long and 1.0 m wide. In Fig. 10a, the novel dynamic PCM wall system is located in the middle of the room bottom. In Fig. 10b, it is located between two windows in the south wall at a height of 1.0 m above the ground. In Fig. 10c, it is located at the lower right corner of wall. In Fig. 10d, it is located between two windows at a distance of 1.6 m from the ground. In Fig. 10e, it is located directly below the right window in the south wall.

Figure 11 shows indoor temperature of the novel PCM wall system at different locations in the wall. In order to clearly show the temperature trend of the room, the temperature of the center point in the room was plotted. As shown in the figure, from 17:00 to 20:00, the room temperature was maintained at 303 K for the five positions. Under Tianjin climate,

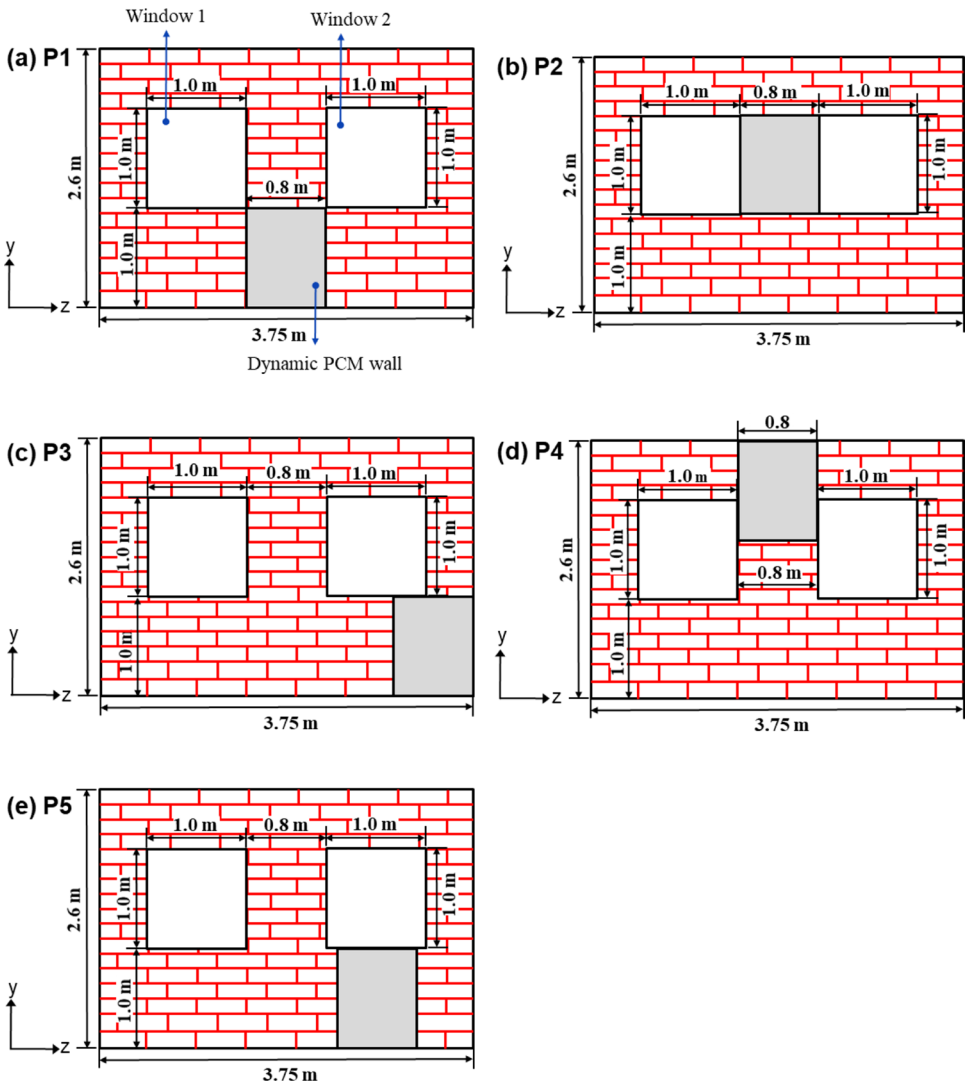

Fig.10 Positions of the novel PCM wall on the south wall of the room

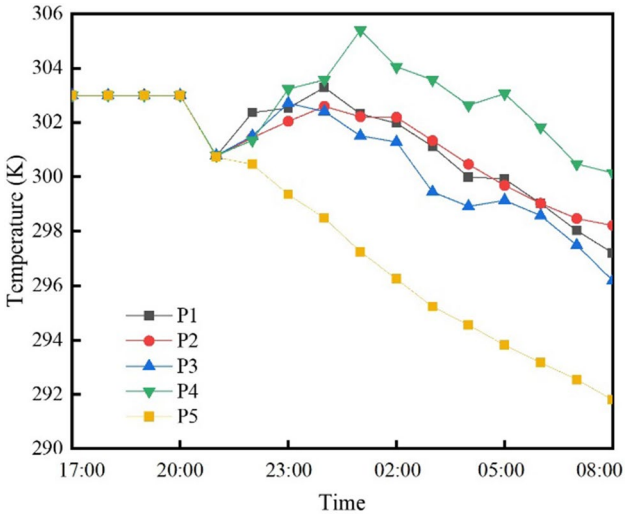

Fig.11 Indoor temperature of the novel PCM wall system at different locations in the wall

PCM has been kept in liquid state from 17:00 to 20:00, so HVAC system will be used for heating during this period, and the temperature will be maintained at 303 K. After 20 o 'clock, PCM began to solidify, so HVAC system was turned off. From 20:00 to 21:00, PCM was at the beginning of solidification, releasing less latent heat, which was not enough to maintain the room temperature, and the room temperature dropped. After 21:00, the room temperature of the five locations was quite different. Among them, the room temperature of the first four positions (P1 to P4) increased after 21:00, and reached the peak at about 24:00, 24:00, 23:00 and 1:00, and then decreased. In the last position (P5), the room temperature had been decreasing after 21:00. The results showed that the position of the PCM system can affect the indoor temperature by changing the heat absorption and diffusion.

Figure 12 showed 2D images of room temperatures in five different PCM positions in Tianjin. The position of the plane was shown in Fig. 9. As shown in Fig. 12, due to the difference of cold and hot air density, the temperature of the upper part of the room was higher than that of the lower part. And the scope of human activity is mainly concentrated in the middle and lower parts of the room, so the temperature of this part determines comfort level. Overall, the temperatures at the five locations were P4, P2, P1, P3 and P5 from high to low. In terms of comfort temperature, the temperature of the lower half room in P4 can be maintained at about 301 K for the longest time, which is the most suitable for human activities among the five cases.

5 Conclusions

Based on the novel dynamic PCM wall system proposed, numerical simulation was conducted. In order to explore the optimal operating conditions of the system, climatic condition, room size design and PCM location were optimized and analyzed. Results of the analyses support the following conclusions:

1. The dynamic PCM wall used in different climate condition in February was simulated and the results showed that in the charging process, the PCM could all melt in the city of Tianjin, Jinan and Guangzhou. In Harbin, it could melt about 60%. In the discharging process, the PCM could only all solidified in north city of Harbin, Tianjin and lasted for about 6 and 9 h respectively. This demonstrated the application potential in cold winter weather. Further research is needed in Harbin city or Jinan city by adjusting the thickness and position of PCM or building design, etc. to promote PCM's thermal behavior.
2. For room size design, view the optimization results, the size of 6 m × 3.25 m × 2.6 m (R1) had the best thermal performance among the four designs, which can maintain the temperature in comfort range for the longest time.
3. As for the position of PCM layer in the north facing wall, five typical locations were selected for optimization. The position of PCM layer affected its heat dissipation. So the PCM thermal performance was also related to the heat dissipation of the PCM location. The results revealed that there was obvious difference in thermal properties at different positions of the PCM layer.

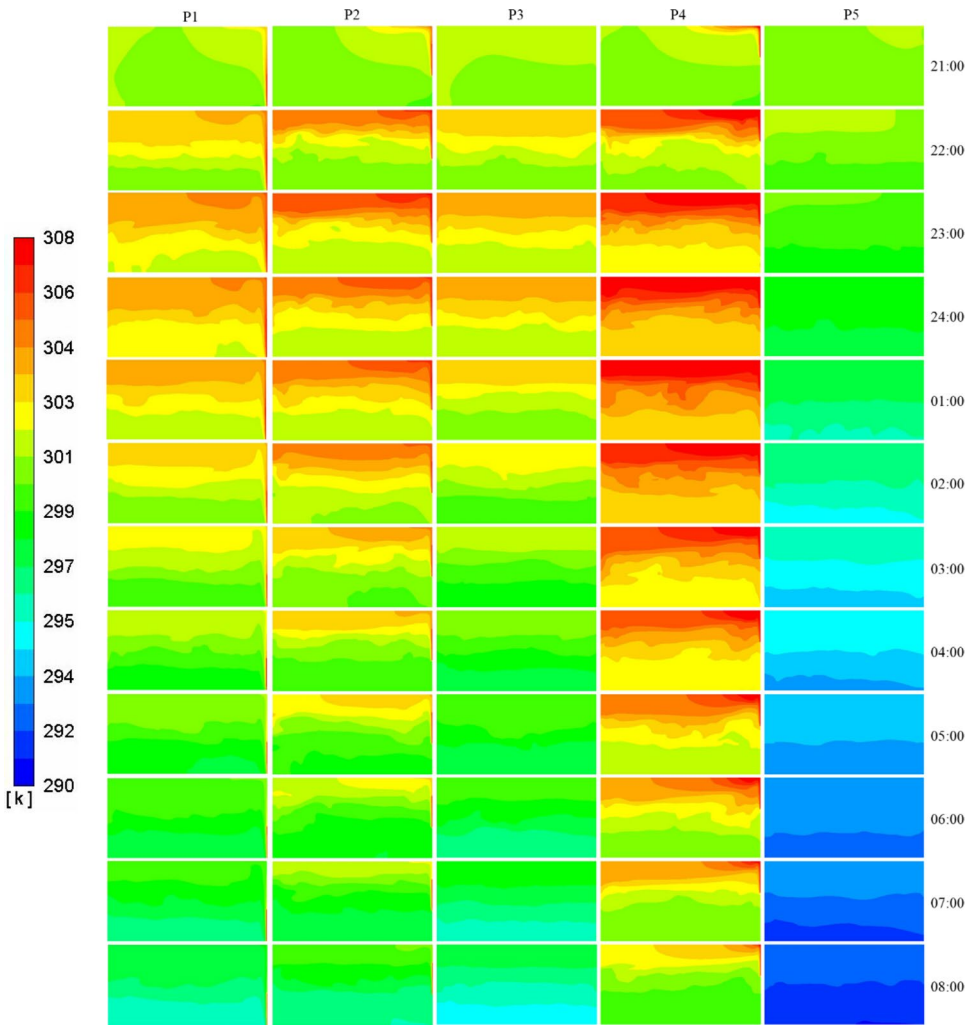

Fig.12 Temperature profile of room with different PCM positions in Tianjin

4. Overall, the phase change materials selected in this study have the potential for heat release in winter, but not all climate conditions can result in the best performance of phase change materials. It is very important to increase the heat release time of phase change materials in order to maintain indoor temperature through the use of new dynamic phase change material walls.
5. Relatively speaking, from the shape of the room, the smaller the area equipped with PCM walls, the better the indoor insulation effect.
6. The installation position of phase change material walls has a significant impact on the insulation effect. It can be seen that the installation position higher is beneficial for indoor insulation. This may be related to the intensity of solar radiation received at different locations.

Acknowledgements This work was supported by National Natural Science Foundation of China [52100047], which is gratefully acknowledged.

Author contributions GZ, YM and BW wrote the main manuscript text. YM and MW prepared figures. DC revised the manuscript. All authors reviewed the manuscript.

Funding National Natural Science Foundation of China, 52100047

Data availability The datasets generated during and/or analyzed during the current study are available from the corresponding author on reasonable request.

Declarations

Competing interests The authors declare no competing interests.

References

1. IEA, Buildings: A source of enormous untapped efficiency potential. 2019. https://www.iea.org/topics/buildings. Accessed 21 Jul 2020.
2. S.A. Krawietz, Passive Solar Heating Methods for Energy Efficient Architecture, in: DY Goswami, Y. Zhao (Eds). Proceedings of ISES World Congress 2007 (Vol. I–Vol. V), Springer Berlin Heidelberg, Berlin, Heidelberg, 2009, pp. 862–866. (2009).
3. Schnieders J, Feist W, Rongen L. Passive houses for different climate zones. Energy Buil. 2015;105:71–87. https://doi.org/10.1016/j.enbuild.2015.07.032.
4. Zirnhelt HE, Richman RC. The potential energy savings from residential passive solar design in Canada. Energy Build. 2015;103:224–37. https://doi.org/10.1016/j.enbuild.2015.06.051.
5. Baetens R, Jelle BP, Gustavsen A. Phase change materials for building applications: a state-of-the-art review. Energy Build. 2010;42(9):1361–8. https://doi.org/10.1016/j.enbuild.2010.03.026.
6. Dutil Y, Rousse DR, Salah NB, Lassue S, Zalewski L. A review on phase-change materials: mathematical modeling and simulations. Renew Sustain Energy Rev. 2011;15(1):112–30. https://doi.org/10.1016/j.rser.2010.06.011.
7. Athienitis CLAK, Hawes D, Banu D, D. Feldman, investigation of the thermal performance of a passive solar test-room with wall latent heat storage. Build Environ. 1997;32(5):405–10. https://doi.org/10.1016/S0360-1323(97)00009-7.
8. Barzin R, Chen JJJ, Young BR, Farid MM. Application of PCM underfloor heating in combination with PCM wallboards for space heating using price based control system. Appl Energy. 2015;148:39–48. https://doi.org/10.1016/j.apenergy.2015.03.027.
9. Nghana B, Tariku F. Phase change material's (PCM) impacts on the energy performance and thermal comfort of buildings in a mild climate. Build Environ. 2016;99:221–38. https://doi.org/10.1016/j.buildenv.2016.01.023.
10. Guarino F, Athienitis A, Cellura M, Bastien D. PCM thermal storage design in buildings: experimental studies and applications to solaria in cold climates. Appl Energy. 2017;185:95–106. https://doi.org/10.1016/j.apenergy.2016.10.046.
11. Izquierdo-Barrientos MA, Belmonte JF, Rodríguez-Sánchez D, Molina AE, Almendros-Ibáñez JA. A numerical study of external building walls containing phase change materials (PCM). Appl Therm Eng. 2012;47:73–85. https://doi.org/10.1016/j.applthermaleng.2012.02.038.
12. Lagou A, Kylili A, Šadauskienė J, Fokaides PA. Numerical investigation of phase change materials (PCM) optimal melting properties and position in building elements under diverse conditions. Constr Build Mater. 2019;225:452–64. https://doi.org/10.1016/j.conbuildmat.2019.07.199.
13. Jin X, Medina MA, Zhang X. On the importance of the location of PCMs in building walls for enhanced thermal performance. Appl Energy. 2013;106:72–8. https://doi.org/10.1016/j.apenergy.2012.12.079.
14. Yu J, Yang Q, Ye H, Luo Y, Huang J, Xu X, Gang W, Wang J. Thermal performance evaluation and optimal design of building roof with outer-layer shape-stabilized PCM. Renew Energy. 2020;145:2538–49. https://doi.org/10.1016/j.renene.2019.08.026.
15. de Gracia A. Dynamic building envelope with PCM for cooling purposes—proof of concept. Appl Energy. 2019;235:1245–53. https://doi.org/10.1016/j.apenergy.2018.11.061.
16. Devaux P, Farid MM. Benefits of PCM underfloor heating with PCM wallboards for space heating in winter. Appl Energy. 2017;191:593–602. https://doi.org/10.1016/j.apenergy.2017.01.060.
17. Bhamare DK, Rathod MK, Banerjee J. Numerical model for evaluating thermal performance of residential building roof integrated with inclined phase change material (PCM) layer. J Build Eng. 2020. https://doi.org/10.1016/j.jobe.2019.101018.
18. Yu J, Leng K, Ye H, Xu X, Luo Y, Wang J, Yang X, Yang Q, Gang W. Study on thermal insulation characteristics and optimized design of pipe-embedded ventilation roof with outer-layer shape-stabilized PCM in different climate zones. Renew Energy. 2020;147:1609–22. https://doi.org/10.1016/j.renene.2019.09.115.
19. Jin X, Zhang X. Thermal analysis of a double layer phase change material floor. Appl Therm Eng. 2011;31(10):1576–81. https://doi.org/10.1016/j.applthermaleng.2011.01.023.
20. Markarian E, Fazelpour F. Multi-objective optimization of energy performance of a building considering different configurations and types of PCM. Sol Energy. 2019;191:481–96. https://doi.org/10.1016/j.solener.2019.09.003.
21. Yang YK, Kim MY, Chung MH, Park JC. PCM cool roof systems for mitigating urban heat island—an experimental and numerical analysis. Energy Build. 2019. https://doi.org/10.1016/j.enbuild.2019.109537.
22. Mahdaoui M, Hamdaoui S, Ait Msaad A, Kousksou T, El Rhafiki T, Jamil A, Ahachad M. Building bricks with phase change material (PCM): Thermal performances. Constr Build Mater. 2021. https://doi.org/10.1016/j.conbuildmat.2020.121315.
23. Voller VR, Prakash C. A fixed grid numerical modelling methodology for convection-diffusion mushy region phase-change problems. Int J Heat Mass Transfer. 1987;30(8):1709–19. https://doi.org/10.1016/0017-9310(87)90317-6.
24. ANSYS Fluent User's Guide. Release 14.5. Canonsburg: ANSYS Inc.,; 2012.
25. Cabeza LF, Castell A, Barreneche C, de Gracia A, Fernández AI. Materials used as PCM in thermal energy storage in buildings: a review. Renew Sustain Energy Rev. 2011;15(3):1675–95. https://doi.org/10.1016/j.rser.2010.11.018.

26. Pirasaci T. Investigation of phase state and heat storage form of the phase change material (PCM) layer integrated into the exterior walls of the residential-apartment during heating season. Energy. 2020;207:118176. https://doi.org/10.1016/j.energy.2020.118176.
27. Chen J, Yang D, Jiang J, Ma A, Song D. Research progress of phase change materials (PCMs) embedded with metal foam (a Review), Procedia. Mater Sci. 2014;4:389–94. https://doi.org/10.1016/j.mspro.2014.07.579.
28. Li ZX, Al-Rashed AAAA, Rostamzadeh M, Kalbasi R, Shahsavar A, Afrand M. Heat transfer reduction in buildings by embedding phase change material in multi-layer walls: Effects of repositioning, thermophysical properties and thickness of PCM. Energy Convers Manage. 2019;195:43–56. https://doi.org/10.1016/j.enconman.2019.04.075.
29. ASHRAE. https://www.ashrae.org/. Accessed 18 Oct 2020
30. Pasupathy A, Athanasius L, Velraj R, Seeniraj RV. Experimental investigation and numerical simulation analysis on the thermal performance of a building roof incorporating phase change material (PCM) for thermal management. Appl Therm Eng. 2008;28(5–6):556–65. https://doi.org/10.1016/j.applthermaleng.2007.04.016.